IL NUOVO CIMENTO **45 C** (2022) 23
DOI 10.1393/ncc/i2022-22023-x

COLLOQUIA: SoUP 2021

# Estimation of muon induced background event rate of AMoRE-II

J. SEO(1), E. J. JEON(2) and M. H. LEE(1)(2)

(1) *IBS School, University of Science and Technology (UST) - Daejeon, South Korea*
(2) *Center for Underground Physics, Institute for Basics Science (IBS) - Daejeon, South Korea*

received 4 November 2021

**Summary.** — The AMoRE-II is the next phase of the AMoRE searching for the neutrinoless double beta decay of $^{100}$Mo isotopes. One of the dominant background sources in the underground experiments are cosmic muons. This study estimated the muon induced background rates with different shield configurations using Geant4 simulation packages. Details of the various shield configurations and their effects on vetoing of muons and muon induced background events are discussed.

## 1. – Introduction

Advanced Mo-based Rare process Experiment (AMoRE) [1-3] is preparing the second phase for the neutrinoless double beta ($0\nu\beta\beta$) decay of $^{100}$Mo isotopes using about 200 kg of molybdenum containing cryogenic detectors. In order to achieve the maximum sensitivity, the AMoRE is aiming to achieve zero-background. One of the methods for reducing the background is to have the experiment to be carried in a deep underground, free from the cosmic ray backgrounds. Thus, the AMoRE-II is being prepared to run at Yemilab located at the Handuk mine near Yemi mountain, Jeongseon, South Korea, with 1000 m depth. However, there are still survived cosmic muons that can affect the measurement and should be excluded as much as possible. This study aims to estimate the muon-induced background rates for different AMoRE-II shield configurations and confirm that the AMoRE-II goal of $< 10^{-5}$ counts/keV/kg/year (ckky) in the region of interest (ROI), $2.8 \sim 3.2$ MeV, can be achieved. The ROI is determined considering the energy range based on the energy resolution of the detector [4,5] for the Q value of $0\nu\beta\beta$ decay of $^{100}$Mo in molybdate crystals, 3034.40(17) keV [6].

## 2. – Geant4 simulation

**2˙1.** *Cosmic muon and muon-induced background.* – For the background studies, we performed the Monte Carlo simulations. The muon background source was simulated using the Geant4 toolkit, version 10.5 [7]. In order to improve the speed and precision

 

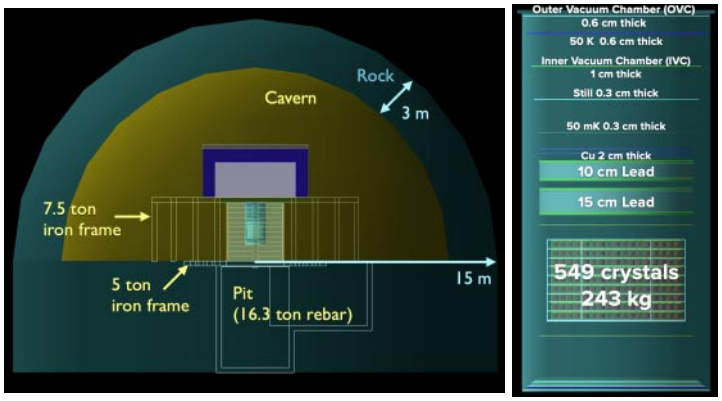


(a) (b)

Fig. 1.: Detector overviews in the cavern (a) and in the outer vacuum chamber (OVC) (b).

of the hadron simulations, we customized the AMoRE-specific physics list [8]. We generated muons at the outer surface of the rock shell surrounding the cavern. With this, all the primary and secondary particles induced by muon interaction with rock can be considered. The energy distribution used for generating muons was obtained by calculating the energy of a muon traveling a certain distance inside the rock using the average energy loss. This calculation was done based on the assumption that muon travels in the same direction until it reaches the underground laboratory [8, 9]. The estimated muon flux at Yemilab is $8.2 \times 10^{-8}$ muons/cm$^2$/s which is derived by the measured flux of 328 $\pm$ 1(stat.) $\pm$ 10(syst.) muons/m$^2$/day by the COSINE-100 experiment at the Yangyang underground laboratory (Y2L) [8, 10].

**2**˙2. *AMoRE-II simulation geometry.* – Figure 1(a) shows an overview of the underground laboratory used in the simulation. In order to see the muon interaction in the rock, a 3 m thick rock volume was added surrounding the cavern. The rock thickness was optimized based on another simulation reported in ref. [8]. There are 8 tons of iron frame and 16.3 tons of rebar in the pit to check the effect of muon-induced neutron capture events. The cross-sectional view of the cryostat is shown in fig. 1(b). The cryostat is composed of a stainless still chamber (Outer Vacuum Chamber, OVC) and four layers of copper chambers (50 K, 4 K, 1 K, and 50 mK). Inside the 50 mK chamber, there are 549 calcium molybdate ($^{40}$Ca$^{100}$MoO$_4$, CMO) crystals. The crystals are arranged in 61 towers, and each tower has nine crystal modules. Finally, 10 and 15 cm thick lead shields are located above the CMO crystal array. Each lead shield is supported by two 2 cm thick copper plates on the upper and lower parts.

We have studied the muon and muon-induced background events with three different shield configurations as shown in figs. 2(a)–(c). The shield for the area surrounding the cryostat consists of 3 cm thick Plastic Scintillator (PS) for muon veto, 70 cm thick polyethylene, 1.5 cm thick borated polyethylene, 25 cm thick lead, and 1 cm thick boric acid rubber, from outside to inside. Differences between the configurations for the lower part is the PS. The PS in configuration 1 is an ideal single volume. However, for configurations 2 and 3, it is divided by 126 modules which have two layers of plastic scintillators as shown in fig. 2(d). The shield for the upper part of cryostat in configuration 1 consists

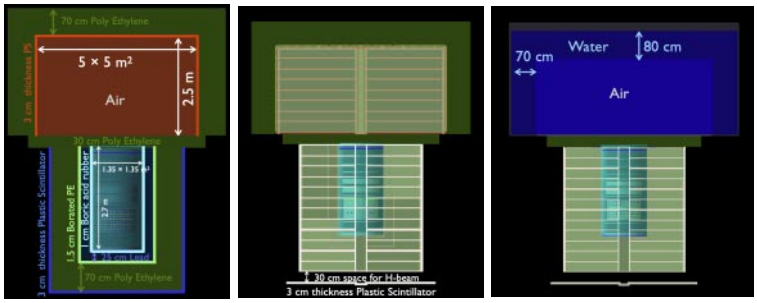


(a) Configuration 1. (b) Configuration 2. (c) Configuration 3.

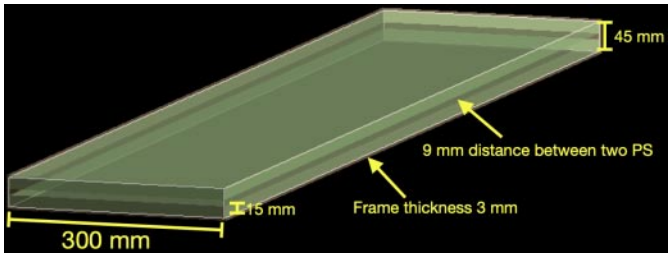


(d) Muon veto panel.

Fig. 2.: Three shield design configurations ((a)–(c)) and a muon veto panel (d).

of 70 cm thick polyethylene and 3 cm thick PS. In configuration 2, the plastic scintillators for both upper and lower shield parts are divided into smaller panels, 106 for the upper and 126 for the lower part. There are H-beam structures in a 30 cm gap between the shield and bottom plastic scintillators to support the AMoRE detector. For configuration 3, the upper part is made of a water tank with 70 cm thick side structure and 80 cm thick top structure because of Photo Multiplier Tubes (PMTs). The lower part is the same as that in configuration 2.

## 3. – Muon tagging and vetoing by plastic scintillator

We performed the analysis in the following steps: 1) Single hit event selection 2) Muon event tagging using the deposited energies in plastic scintillators 3) Muon event vetoing using the time information. The first requirement of the event selection is the rejection of the multiple crystal hits in an event. Most background events can deposit their energies in multiple crystals, while the double beta decay events can deposit in a single crystal due to the short ranges of the emitted electrons [5]. In this study, each simulated event has a 100 ms event window. Thus, only events with their deposited energy in a single crystal within this event window were selected for analysis. Then we tag the muon events using energy information in the plastic scintillator(s) and water tank. Figures 3(a)–(c) show the deposited energies in the plastic scintillator(s) and water tank for different configurations. We set the energy threshold where the muon peak begins. Finally, we select the event using timing information. Figure 4 shows the time difference between a plastic scintillator hit and a crystal hit. Most of the events are in a 2 ms time difference between plastic scintillator and crystal hit. In this study, we set the veto time window at 5 ms.

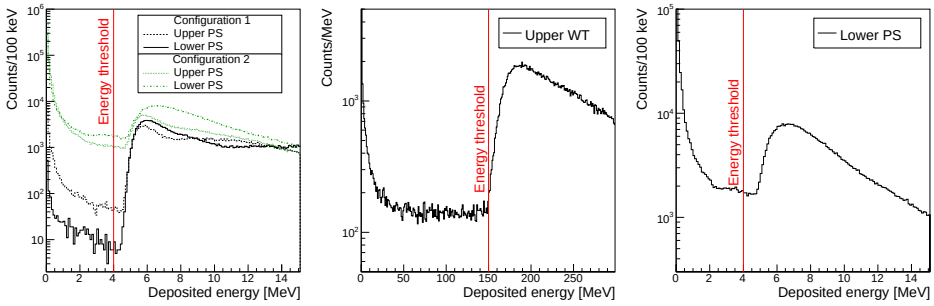


(a) Configurations 1 and 2. (b) Configuration 3 WT. (c) Configuration 3 PS.

Fig. 3.: Deposited energies in plastic scintillator and water tank for three different configurations.

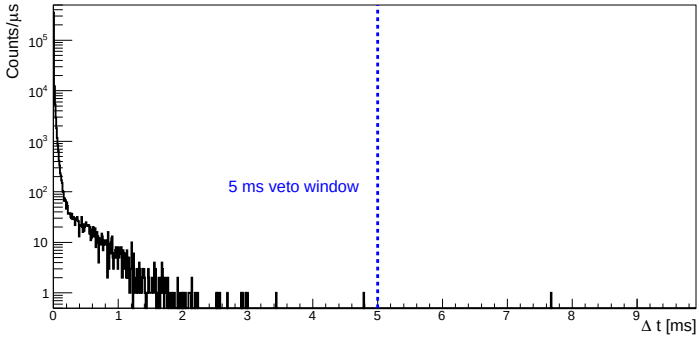


Fig. 4.: A distribution of time difference ($\Delta$t) between single crystal hit and PS hit(s) or WT hit after the single hit selection.

## 4. – Result

Figure 5 shows the deposited energy distributions in the crystals. The single hit background events before applying the muon event veto are shown by the black-dashed lines. The energy distributions represented by the green lines are for survived events after vetoing the muon events using lower muon veto detector(s). The red-filled areas represent the background events surviving the veto of upper and lower muon veto detector(s). The estimated background event rates in ROI are summarized in table I. For configuration 1, the single hit background event rate is $1.65 \times 10^{-3}$ ckky. There is no background event in ROI when the muon event is vetoed by the upper and lower veto detectors together, and the estimated upper limit is $< 2.24 \times 10^{-6}$ ckky (90% C.L. [11]). As expected, the background event rates for configurations 2 and 3 are a little bit increased compared to that for the configuration 1. The estimated background event rates after vetoing with upper and lower veto detector are the same with $2.75 \times 10^{-6}$ ckky for both configurations.

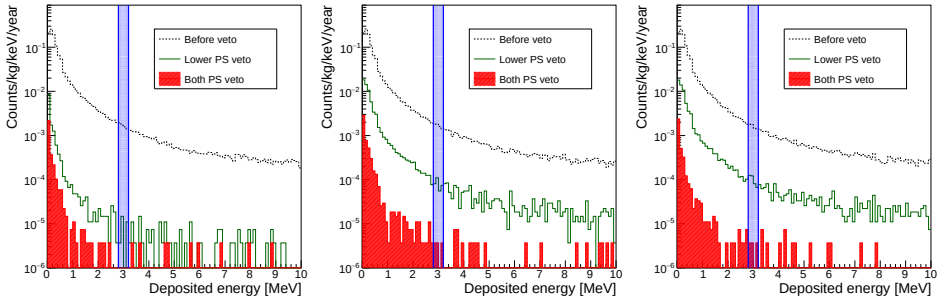


(a) Configuration 1. (b) Configuration 2. (c) Configuration 3.

Fig. 5.: Deposited energies in the crystals for three different configurations.

TABLE I.: The background event rates in three configurations for different veto conditions.

Unit: $\times 10^{-3}$ ckky

| Veto condition | Configuration 1 | Configuration 2 | Configuration 3 |
|---|---|---|---|
| Before | $1.65 \pm 0.0390$ | $1.66 \pm 0.0390$ | $1.61 \pm 0.0384$ |
| Lower | $0.00734 \pm 0.00259$ | $0.0799 \pm 0.00856$ | $0.0982 \pm 0.00950$ |
| Upper+Lower | $< 0.00224$ (90% C.L.) | $0.00275 \pm 0.00159$ | $0.00275 \pm 0.00159$ |

## 5. – Conclusion

We performed simulations and analysis of the muon induced background events for the three different configurations of the muon veto detector system in the AMoRE-II. The estimated event rate for configuration 1 with an ideal plastic scintillator is $2.24 \times 10^{-6}$ ckky. Configurations 2 and 3 with segmented plastic scintillators (2) and a water tank in the upper part (3) show the estimated event rate $2.75 \times 10^{-6}$ ckky for both. All configurations of the muon veto detectors in this work can achieve AMoRE's goal ($< 10^{-5}$ ckky). The designs for the muon veto system in the AMoRE-II keeps being developed by considering the use of the water Cherenkov detector as a muon veto system.

## REFERENCES

[1] BHANG H. *et al.*, *J. Phys.: Conf. Ser.*, **375** (2012) 042023.
[2] ALENKOV V. *et al.*, arXiv:1512.05957 (2015).
[3] LEE M. H., *JINST*, **15** (2020) C08010.
[4] KIM G. B. *et al.*, *Adv. High Energy Phys.*, **2015** (2015) 817530.
[5] ALENKOV V. *et al.*, *Eur. Phys. J. C*, **79** (2019) 791.
[6] RAHAMAN S., ELOMAA V. V., ERONEN T. *et al.*, *Phys. Lett. B*, **662** (2008) 111.
[7] AGOSTINELLI S. *et al.*, *Nucl. Instrum. Methods Phys. Res. A*, **506** (2003) 250.
[8] BAE H. W., JEON E. J. *et al.*, *Astropart. Phys.*, **114** (2020) 60.
[9] REICHENBACHER J., in *Proceedings of the 30th International Cosmic Ray Conference*, Vol. **5** (Universidad Nacional Autonoma de Mexico) 2007, p. 1241.
[10] PRIHTIADI H. *et al.*, *JINST*, **13** (2018) T02007.
[11] LUQMAN A. *et al.*, *Nucl. Instrum. Methods Phys. Res. A*, **855** (2017) 140.